

Verification of conditional mechanical squeezing for a mg-scale pendulum near quantum regimes

Jordy G. Santiago-Condori^a, Naoki Yamamoto^b, and Nobuyuki Matsumoto^c

^aResearch Institute of Electrical Communication, Tohoku University, Sendai 980-8577, Japan

^bDepartment of Applied Physics and Physico-Informatics, Keio University, Hiyoshi 3-14-1, Kohoku, Yokohama 223- 8522, Japan

^cDepartment of Physics, Gakushuin University, Mejiro 1-5-1, Toshima, Tokyo 171-8588, Japan

November 16, 2023

E-mail: matsumoto.granite@gmail.com

Abstract

In quantum mechanics, measurement can be used to prepare a quantum state. This principle is applicable even for macroscopic objects, which may enable us to see classical-quantum transition. Here, we demonstrate conditional mechanical squeezing of a mg-scale suspended mirror (i.e. the center-of-mass mode of a pendulum) near quantum regimes, through continuous linear position measurement and quantum state prediction. The experiment involved the pendulum interacting with photon coherent fields in a detuned optical cavity, which creates an optical spring. Furthermore, the detuned cavity allows us to perform linear position measurement by direct photo-detection of the reflected light. We experimentally verify the conditional squeezing using the theory combining prediction and retrodiction based on the causal and anti-causal filters. As a result, the standard deviation of position and momentum are respectively given by 36 times the zero-point amplitude of position q_{zpf} and 89 times the zero-point amplitude of momentum p_{zpf} . The squeezing level achieved is about 5 times closer to the zero-point motion, despite that the mass of the mechanical oscillator is approximately 7 orders of magnitude greater, compared to the previous study. Thus, our demonstration is the first step towards quantum control for massive objects whose mass-scale is high enough to measure gravitational interactions. Such quantum control will pave the way to test quantum mechanics using the center-of-mass mode of massive objects.

Introduction

The investigation of continuous linear position measurements of macroscopic objects has been mainly motivated by the direct detection of gravitational waves [1, 2], and the field of cavity optomechanics [3]. These research established the standard quantum limit (SQL) for continuous position measurements [4, 5], where shot noise and quantum back-action noise contribute equally. Such precise measurements allow measurement-based quantum control of macroscopic objects, like ground state cooling [6, 7, 8] and generation of entanglement [9, 10], since correlations are built up between the mechanical objects and the measuring devices via radiation pressure of light. It is expected that, as the measurement sensitivity increases for example by enhancing the mechanical quality factor [11, 12, 13, 14], tests with quantum oscillators of unexplored phenomena such as gravity decoherence [15, 16, 17, 18, 19, 20], semiclassical gravity [21, 22, 23], and dark matter-induced fifth force [24, 25, 26] will become possible. One of the most challenging tasks is to measure entanglement via Newtonian gravity in order to test the quantum nature of the gravitational interaction [27, 28, 29, 30, 31]. Towards this ultimate end, it is important to first develop technology to control the center-of-mass mode of massive objects via laser light.

Recently, Meng *et al.* [32, 33] demonstrated theoretically and experimentally that mechanical squeezing can be generated outside the rotating wave approximation regime, by applying a causal Wiener filter [34], which minimizes the mean-square estimation error for position monitoring. While in [32] Meng *et al.* consider an optomechanical system consisting of an optical cavity on resonance coupled to a mechanical oscillator, in our analysis we take into account a detuning from resonance. This is because a detuned cavity allows us to create an optical spring [35, 11, 36] that optically traps a massive mechanical oscillator of low rigidity (e.g. the pendulum mode of a suspended mirror). Importantly, this lets us sufficiently increase the quantum coherence time of the mechanical mode [37]. Furthermore, the detuned cavity allows us to monitor the position via direct photo-detection, which is the simplest configuration among various optical detection schemes, such as homodyne detection. Because generation of entanglement normally requires the use of a complex Power-Recycling Fabry-Perot Michelson Interferometer (PRFPMI) [9, 10], simplifying the detection system is extremely important to increase the feasibility of the experiment.

In this paper, we derive the analytic solution of a causal Wiener filter for preparing conditional squeezing as well as an anti-causal Wiener filter for verifying the state. Since conditional states are characterized by conditional variances (the mean of the squared difference between the *true* value and the estimated value by the causal filter), it requires us to obtain experimental access of the true value for determining the state. This *true* value, on the other hand, is only available mathematically, especially in case where the system is macroscopic. To avoid this difficulty, we experimentally verify conditional variances by comparing the results of causal and anti-causal estimation following Rossi *et al* [38]. According to this process, the conditional state can be verified only by using the measured data and the filters including system parameters, independent of quantum physical properties such as position and momentum.

Here, we present experimental verification for the conditional squeezing in the center-of-mass of an optically trapped mg-scale pendulum (resonance at 280 Hz) near quantum regimes, by applying causal and anti-causal Wiener filters to the position measurement record previously reported for gravity sensing [39]. The verified position (momentum) standard deviation is 36 (89) times the zero-point amplitude q_{zpf} (p_{zpf}). This is, to the best of our knowledge, the first experimental demonstration of mechanical squeezing near quantum regimes using a macroscopic pendulum, whose mass-scale is high enough to measure gravitational interactions [39, 40].

Theory for conditional squeezing

We consider a detuned cavity comprised of a pendulum of mass m under feedback cooling, as shown in Fig. 1. Laser light enters the cavity and receives an intensity shift proportional to the mechanical position, which is read out via direct photo detection and fed back to the pendulum for cooling [41]. We analyze the linearized Hamiltonian in a rotating frame at the laser frequency ω_L , given by $H = \hbar\Omega(q^2 + p^2)/4 - \hbar\Delta(x^2 + y^2)/4 + \hbar g x q$. Here, \hbar is the reduced Planck constant, Δ is the detuning of the optical cavity, $\Omega/2\pi$ is the bare mechanical resonance frequency, x (y) is the dimensionless amplitude (phase) quadrature of the light, and q (p) is the dimensionless position (momentum) of the mechanical oscillator. $g \equiv G\sqrt{n_c}\sqrt{\hbar/2m\Omega}$ is the light-enhanced optomechanical coupling constant [42], where G is the optical frequency shift per displacement, and n_c is the number of photons circulating inside the cavity. The commutation relations are normalized as $[x, y] = [q, p] = 2i$, resulting in the variance of each zero point motion to unity.

Under the adiabatic limit ($\kappa \gg \omega$) and considering a small detuning $\Delta \ll \kappa$, we obtain the following quantum Langevin equations by adiabatically eliminating the cavity mode:

$$\begin{aligned} \dot{q} &= \omega_m p, \\ \dot{p} &= -\omega_m q - \gamma_m p + \sqrt{2\gamma_m} p_{\text{in}} - \frac{4g_m}{\sqrt{\kappa}} x_{\text{in}} + \frac{8g_m\delta}{\sqrt{\kappa}} y_{\text{in}}, \\ X &= -\frac{8g_m\delta\sqrt{\eta}}{\sqrt{\kappa}} q - \sqrt{\eta} x_{\text{in}} + 4\delta\sqrt{\eta} y_{\text{in}}. \end{aligned} \quad (1)$$

Here, κ is the optical decay rate, ω_m is the mechanical resonance trapped in the optical potential, γ_m is the mechanical decay rate under cooling, and $g_m \equiv g\sqrt{\Omega/\omega_m} = G\sqrt{n_c}x_{zpf}$ is the coupling constant for the trapped mode. Further, $\delta \equiv \Delta/\kappa$ is the normalized detuning, X is the measured

optical amplitude quadrature with the detection efficiency η , and x_{in} and y_{in} (p_{in}) refer to the optical (mechanical) noise input satisfying $\langle x_{\text{in}}^2 \rangle = \langle y_{\text{in}}^2 \rangle = 2N_{\text{th}} + 1$ ($\langle p_{\text{in}}^2 \rangle = 2n_{\text{th}} + 1$), where N_{th} (n_{th}) is the thermal phonon number in light (the unconditional occupation under feedback cooling). From the third equation in Eq. (1), we can see that the measurement of light intensity can clearly provide linear continuous measurement of the position q , which induces the conditional mechanical squeezing of q ; note that the quality of squeezing depends on the sensitivity coefficient defined by $A \equiv -8g_m\delta\sqrt{\eta}/\sqrt{\kappa}$ and the sensing (imprecision) noise components due to the optical noises. Note also that q (p) is renormalized by a factor of $\sqrt{\Omega/\omega_m}$ ($\sqrt{\omega_m/\Omega}$) by taking into account the change in the resonance frequency by the optical spring.

To discuss how to evaluate the conditional squeezed state, we begin with describing the causal Kalman filter, which computes the least mean-square error estimate $\vec{q}(t)$ of the true value $q(t)$. $\vec{q}(t)$ is the expectation value conditioned on the measurement record (namely, $\vec{q}(t) \equiv E[q(t)|X(s), 0 \leq s \leq t]$), which can be seen as *prediction* of the true value $q(t)$, based on the past data $\{X(s)|0 \leq s \leq t\}$. The dynamics of the predicted value depends on the measurement record $X(t)$ and the conditional variance according to the Riccati equation [43, 44]. When in a steady state, in the Fourier domain with the convention $F(\omega) = \int_{-\infty}^{\infty} f(t) \exp(i\omega t) dt$, the predicted value is calculated as $\vec{q}(\omega) = \vec{H}_q(\omega)X(\omega)$, where $\vec{H}_q(\omega)$ is the causal Wiener filter:

$$\vec{H}_q(\omega) = \frac{1}{\sqrt{\lambda_X M}} \frac{(\omega_X^2 - \omega_m^2) - i\omega(\gamma_X - \gamma_m)}{F'(\omega)}. \quad (2)$$

Here, $1/F'(\omega) = 1/(\omega_X^2 - \omega^2 - i\omega\gamma_X)$ is a modified mechanical susceptibility, with resonance frequency $\omega_X = \sqrt[4]{\omega_m^4 + 2\Lambda_X\omega_m^3 + \Gamma\lambda_X\omega_m^2}$ and decay rate $\gamma_X = \sqrt{\gamma_m^2 - 2\omega_m(\omega_m + \Lambda_X) + 2\omega_X^2}$. λ_X is the measurement rate which determines the inverse time scale to resolve the zero-point fluctuation, $M = 2\eta N_{\text{th}} + 1$ is the total sensing noise, Λ_X is related to the magnitude of back-action, and Γ is the mechanical heating rate. The causal Wiener filter for the momentum, $\vec{H}_p(\omega)$, is given in Supplemental Material. The Wiener filter is the frequency-domain representation of the quantum Kalman filter based on the Langevin equation (1), which maintains the Heisenberg uncertainty relation between q and p , and x and y .

The above state prediction procedure leads to quantum squeezing in the sense that the conditional variances satisfy $\langle (q(t) - \vec{q}(t))^2 \rangle < 1 < \langle (p(t) - \vec{p}(t))^2 \rangle$. However, in quantum mechanics, the true values $(q(t), p(t))$ can never be experimentally determined. To circumvent this essential difficulty and to experimentally verify the prepared conditional squeezing, we calculate the conditional state using the anti-causal filter in addition to the above-described causal filter. This process, known as *retrodiction* [38], computes the estimate $\overleftarrow{q}(t)$ for the true value $q(t)$ using the future data $\{X(s)|t \leq s \leq T\}$ after the entire measurement process is complete. Using the Kalman filter and the associated Riccati equation in an anti-causal manner, we can derive the frequency-domain retrodiction as $\overleftarrow{q}(\omega) = \overleftarrow{H}_q(\omega)X(\omega)$, where $\overleftarrow{H}_q(\omega)$ is the anti-causal Wiener filter:

$$\overleftarrow{H}_q(\omega) = \frac{1}{\sqrt{\lambda_X M}} \frac{(\omega_X^2 - \omega_m^2) + i\omega(\gamma_X + \gamma_m)}{F'(\omega)^*}. \quad (3)$$

Then, the conditional variance for the position, V_{11} , can be determined by comparing the results of prediction and retrodiction filters as follows;

$$\int_{-\infty}^{\infty} \frac{1}{2\pi} (|\overleftarrow{H}_q(\omega)|^2 - |\vec{H}_q(\omega)|^2) S_{XX}(\omega) d\omega \approx 2V_{11}. \quad (4)$$

$S_{\overleftarrow{q}\overleftarrow{q}}(\omega) = |\overleftarrow{H}_q(\omega)|^2 S_{XX}(\omega)$ and $S_{\vec{q}\vec{q}}(\omega) = |\vec{H}_q(\omega)|^2 S_{XX}(\omega)$ are the power spectral density (PSD) of $\overleftarrow{q}(t)$ and $\vec{q}(t)$, respectively, where $S_{XX}(\omega)$ is the PSD of $X(t)$. Similarly, the conditional variance for the momentum, V_{22} , is calculated as

$$\int_{-\infty}^{\infty} \frac{1}{2\pi} (|\overleftarrow{H}_p(\omega)|^2 - |\vec{H}_p(\omega)|^2) S_{XX}(\omega) d\omega \approx 2V_{22}. \quad (5)$$

From these expressions, we can experimentally verify the conditional variances and accordingly the conditional squeezing, using the PSDs which can be constructed only from the output time series of $X(t)$. The details of the above discussion, including the validity of the approximation in Eqs. (4) and (5), are given in Supplemental Material.

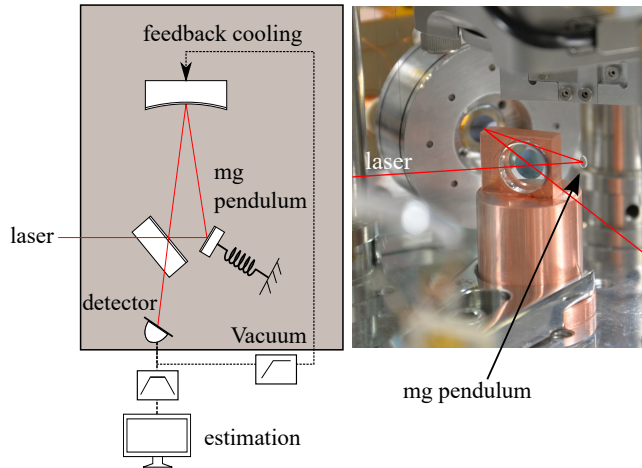


Figure 1: (Color online) Experimental setup. The configuration of the three mirrors can stably trap the mirror's motion [47].

System characterization and position measurement

The optical ring cavity with a cavity decay rate of $\kappa = 2\pi \times 1.64(2)$ MHz consists of a 7.71(1) mg suspended mirror (measured by an accurate electronic balance: AND, BM-5), a 261.42(1) g suspended mirror, and a mirror fixed to a copper monolithic holder with its fundamental resonance at about 10 kHz. The bare mechanical dissipation for the mg pendulum (γ_0) and the heavier pendulum are $\gamma_0 = 2\pi \times 4.74(5) \times 10^{-5}$ Hz and $2\pi \times 1.5 \times 10^{-4}$ Hz, respectively. We can ignore the dynamics of the heavy and fixed mirrors because both have sufficiently small optomechanical coupling and Brownian motion amplitudes.

The intrinsic dissipation of the mg pendulum shows a frequency dependence of $\gamma_0(\omega) \propto \gamma_0(\Omega) \times \Omega/\omega$, which is a characteristic referred to as structural damping [45]. Thus the dissipation at the optical spring resonance frequency decreases as the resonance frequency increases. Note that due to the normal-mode splitting by the optical spring [39, 46], it can be reduced, in our case by a factor of 4. Without modification due to the optical spring and feedback cooling, the bare quality factor given by $\Omega/\gamma_0(\Omega)$ relates the resonance frequency to the magnitude of the thermal force noise ($\propto \gamma_0$). Thus, it can quantify the decoupling of the mechanical resonator from a thermal bath, leading to the number of coherence oscillation before the thermalization given by $\Omega/\gamma_0(\Omega)n_{\text{th}}$ [3]. To observe coherent oscillations more than unity, $Q\Omega > k_B T/\hbar$ should be satisfied, where T is the room temperature. With the modification, the effective quality factor can be defined by $\omega_m/\gamma_0(\omega_m)$ or ω_m/γ_m . In this case, the thermal noise is proportional to $\gamma_m n_{\text{th}}$ as in (4). The value of $\gamma_m n_{\text{th}}$ is independent of the magnitude of feedback cooling because it determines the mechanical heating rate by a thermal bath, while the value of n_{th} can be reduced by feedback. Thus, the number of coherent oscillation is modified to be $\omega_m/\gamma_m n_{\text{th}}$, leading to the condition for observing coherent oscillations given by $\omega_m \omega_m/\gamma_0(\omega_m) > k_B T/\hbar$. In [39] the value of the former quality factor given by $\omega_m/\gamma_0(\omega_m)$ reaches 10^8 , and moreover we show that the number of coherent oscillation can exceed unity within the state-of-the-art technology [13]. On the other hand, the latter quality factor only represents the sharpness of the peak and it is independent of the thermal noise level.

Laser light (Coherent, Mephisto 500) is injected into the cavity with an incident laser power of 30 mW, and the reflected light is directly detected by a photo-detector (HAMAMATSU, G10899-03K) of 92(2) % efficiency. The efficiency is inferred by characterization of the optical spring. Its error includes both the error of the resistance in a current to voltage converter, and that of the incident laser power. To characterize the optomechanical interaction and the detection efficiency, we performed an auxiliary measurement to measure the resonance frequency of the optically trapped pendulum with varying detuning (cyan in Fig. 5 in Supplemental Material). The details of the auxiliary measurement can be found in Section 4 in Supplemental Material. We infer the frequency shift per displacement G to be $-2\pi \times 4.72(3)$ PHz/m and extract the efficiency from the fitting of the measured resonance to

the theory, given in Supplemental Material:

$$\omega_m = \sqrt{\frac{8\hbar G^2 n_c \delta}{(1 + 4\delta^2)\kappa m}}. \quad (6)$$

Figure 2 shows the measured displacement spectrum with the unconditional mode temperature of the optically trapped pendulum of 11(2) mK, which is obtained using Welch’s method [48] with 1.9 Hz resolution and 50% overlap. The phonon number n_{th} is correspondingly $8(2) \times 10^5$, and the quality factor ($\equiv \omega_m/\gamma_m$) is 250(13). This data was calibrated to displacement (the meter-to-voltage conversion factor is $-2.3(4) \times 10^{-10}$ m/V) based on a transfer function analysis, which can be independently derived from the value of the detuning (see Eq. 5 in [41]).

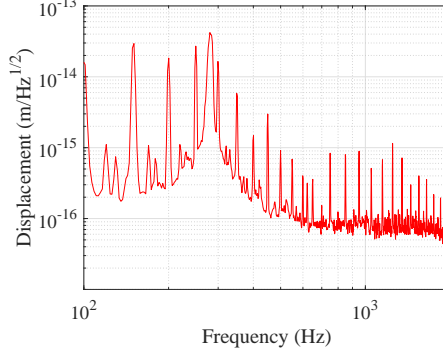


Figure 2: (Color online) The displacement spectrum with the mode temperature of 11 mK (red).

The cavity length was detuned from resonance such that the pendulum’s resonance ($\omega_m/2\pi$) increases to 280(7) Hz. Because of the nonlinearity of the optical spring in Eq. 6 with respect to δ , there are two possible values for the cavity detuning. We determined the value by analysing the data in the time domain (details can be seen in Section 5 in Supplemental Material). As a result, the mean detuning value is about $\Delta = 0.03 \times \kappa$, and the number of photons in the cavity is $1.16(7) \times 10^{10}$, leading to a light-enhanced optomechanical coupling constant g_m of $-2\pi \times 3.2(2) \times 10^4$ Hz. Therefore, we obtain a quantum cooperativity ($C_q \equiv C/n_{\text{th}}$) of 0.0027(8). Furthermore, the sensitivity coefficient obtained is $A = 14(1) \sqrt{\text{Hz}}$. This value is consistent with the meter-to-voltage conversion factor, which is measured independently from the sensitivity coefficient. We also consider contamination in the signal by laser classical noise [39]; The relative intensity noise level is $1.8 \times 10^{-8} / \sqrt{\text{Hz}}$, which is 4.4 times higher than that of the shot noise limit. Thus, this contribution can be modeled as $N_{\text{th}} = 19$. The optomechanical parameters for the optimal state estimation are summarized in Table 1.

Table 1: Optomechanical parameters

Parameter	Value
Mass	$m = 7.71(1)$ mg
Cavity decay rate	$\kappa = 2\pi 1.64(2)$ MHz
Cavity detuning	$\Delta = 0.03 \times \kappa$
Circulating photon number	$n_c = 1.17(6) \times 10^{10}$
Light-enhanced coupling	$g_m = -2\pi 3.2(2) \times 10^4$ Hz
Quantum cooperativity	$C_q = 0.003$
Sensitivity coefficient	$A = 14(1) \sqrt{\text{Hz}}$
Excess noise in the laser	$N_{\text{th}} = 19$

Mechanical squeezing and discussions

Here, we present mechanical squeezing using the data shown in Fig. 2. Firstly, the 50 Hz harmonics from the power supply are rejected by 1st order Butterworth notch filters with a 3 dB stop bandwidth

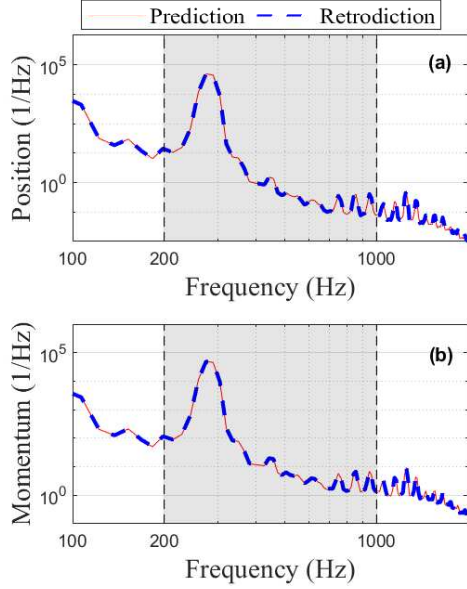


Figure 3: (Color online) PSD normalized by the zero-point amplitude (a) showing the prediction (red) and retrodiction (blue) for displacement. Plot (b) shows the prediction (red) and retrodiction (blue) for momentum. The shaded region represents the region where integration is calculated.

of a few Hertz. Secondly, prediction and retrodiction are performed by multiplying the causal and anti-causal Wiener filters with the dimensionless (non-calibrated) amplitude quadrature X . The result is shown in Fig. 3, where the red lines show the PSD by prediction, $S_{\vec{q}\vec{q}}(\omega)$ and $S_{\vec{p}\vec{p}}(\omega)$; the blue dotted lines show the PSD by retrodiction, $S_{\vec{q}\vec{q}}(\omega)$ and $S_{\vec{p}\vec{p}}(\omega)$. Here, the parameters in the susceptibility of the filters are correspondingly given by $\omega_X = 2\pi \times 704$ Hz and $\gamma_X = 2\pi \times 1073$ Hz. The other terms are respectively $M = 36$, $\Lambda_X = -2\pi \times 578$ Hz, $\lambda_X = 2\pi \times 0.87$ Hz, $\gamma_m = 2\pi \times 1.1$ Hz and $\omega_m = 2\pi \times 280$ Hz. Lastly, we use Eqs. (4) and (5) to calculate the verified conditional variances for position V_{11} and momentum V_{22} as

$$V_{11} = (1.30 \pm 0.32) \times 10^3, \quad (7)$$

$$V_{22} = (8.02 \pm 1.13) \times 10^3. \quad (8)$$

In terms of standard deviation, including the units, each noise level is $36 \times q_{zpf}$ and $89 \times p_{zpf}$. The achieved squeezing level is about 5 times closer to the zero point motion compared to the previous research [33]. Here, the integration is calculated with the range over 200 Hz to 1000 Hz (shown as the shaded regions in Fig. 3) and the frequency resolution of 55 Hz. This frequency bandwidth corresponds to the region where the output equation of $X(t)$ in Eq. (1) is correctly modeled. The first reason of the discrepancy is that our model includes frequency independent PSD of the thermal noise, although the data fits the model given by the structural damping. The effect is especially apparent at frequencies lower than the resonance frequency. The second reason is that our model does not include multi-mode mechanical states such as the pitching mode and violin modes. To overcome the above issues, Meng *et al.* [33] demonstrated to enhance the squeezing level using the multi-mode Wiener filter including the thermal noise model with structural damping. Furthermore, Shichijo *et al.* [49] recently report the derivation of the multi-mode Wiener filter considering the pendulum and rotational modes. Note that the theoretical conditional covariance between q and p , i.e., V_{12} given by Eq. (12) in Supplemental Material, is 2386, corresponding to the squeezing angle of about -18 degrees.

The errors in Eq. (7) in the verification process come from the modeling error. Since the optomechanical parameters are characterized within each specific uncertainties range (refer to Table 1), these uncertainty may serve as the main source of modeling error. To numerically estimate the magnitude of the modeling errors, we conduct a Monte Carlo simulation; that is, we repeatedly generate the state with different parameters that are uniform randomly chosen according to Table 1) in the causal and anti-causal filters with the frequency resolution from 1 Hz to 60 Hz. The results are presented in Fig. 4.

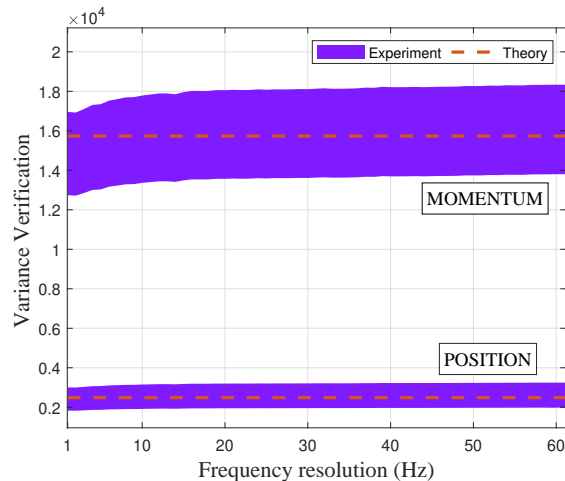


Figure 4: Verification of the conditional mechanical squeezing. The orange dashed lines are the theoretical values of the conditional variances $2V_{11}$ and $2V_{22}$ for the position q and momentum p , respectively. The purple shadows show the range of variances given by the modeling error.

The experimentally verified conditional variances including the modeling errors, given in Eq. (7), agree well with the theory. The tendency for discrepancy between the theory and experiment is observed at resolutions lower than 10 Hz. This is because that the resonance frequency of the pendulum fluctuates about 10 Hz due to fluctuations of the the cavity detuning (see Fig. 6 (c) in Supplemental Material). Since the resonance frequency ω_m is set as a constant in our model, the above fluctuations are not included in the model. Also, in the range beyond 60 Hz in the frequency resolution, the experimentally verified variances diverge, implying that the model is not anymore valid in this frequency regime.

Our demonstration is the first step for generating entanglement between two massive pendulums in a PRFPMI via the radiation pressure of light [9, 10]. To achieve this, the squeezed noise level must be less than the zero-point fluctuation, or in other words, the sensitivity of both the differential and common modes has to reach the SQL in a PRFPMI comprised of two pendulums. In general, interferometers can precisely measure the differential mode through common-mode noise rejection; however, the sensitivity for the common mode decreases significantly due to, e.g., laser frequency noise. Since the result presented here is based on the direct measurement of the center-of-mass mode, it is possible to observe the common mode with the comparable sensitivity if two pendulums are combined in an interferometer. Moreover, we previously reported a monolithically constructed pendulum with lower dissipation [13] that can satisfy the requirement for generating entanglement [10]. Thus, the combination of the low-dissipative oscillator and the mechanical squeezing reported here will result in the generation of an entangled state of mg-scale pendulums, which can be used to probe effects like quantum decoherence of macroscopic objects involving gravitational interactions. The result presented here is also the very first step towards entanglement via Newtonian gravity, in order to test the quantum nature of the gravitational interaction [27, 28, 29, 30, 31].

Conclusion

We analytically derived the causal and anti-causal Wiener filters for a suspended mirror trapped in a detuned optical cavity. By applying these filters to the result of precise displacement measurement by direct photo-detection, we experimentally verified the conditional squeezing with its position variance achieving 1.3×10^3 with an initial occupation of 8×10^5 , in other words, with an initial mode temperature of 11 mK. Since our system can precisely measure displacement of the center-of-mass mode directly without depending on common-mode noise rejection, this research can pave the way to generate quantum entanglement between two massive pendulums in an interferometer, where both the differential and common modes have to be sensed with the SQL sensitivity. In conclusion, the mechanical squeezing presented in this paper is the first step for quantum control of massive oscilla-

tors, especially in entanglement generation between massive pendulums, aiming towards the probing of unexplored phenomena such as gravity decoherence and the quantum nature of the gravitational interaction.

1 The model system

The original system composed of the mechanical oscillator, the optical cavity, and the feedback control is governed by the following quantum Langevin equations:

$$\begin{aligned}\dot{x} &= -\kappa x/2 - \Delta y + \sqrt{\kappa} x_{\text{in}}, \\ \dot{y} &= -\kappa y/2 + \Delta x + \sqrt{\kappa} y_{\text{in}} - 2gq, \\ \dot{q} &= \Omega p, \\ \dot{p} &= -\Omega q - \gamma_0 p + \sqrt{2\gamma_0} p_{\text{in}} - 2gx - \int_{-\infty}^t ds g_{\text{FB}}(t-s) X(s),\end{aligned}$$

where (q, p) are the position and momentum operators of the mechanical oscillator and $a = x + iy$ is the annihilation operator of the cavity mode. Also $\langle x_{\text{in}}^2 \rangle = \langle y_{\text{in}}^2 \rangle = 2N_{\text{th}} + 1$ and $\langle p_{\text{in}}^2 \rangle = 2k_B T / \hbar \Omega + 1$, where T is the room temperature. g_{FB} is a causal high-pass filter for cold damping (i.e. cooling by feedback) [41], which allows us to ignore the dissipative optical force applied on the mechanical oscillator (i.e., the imaginary part of the optical spring). Note that the laser frequency is not locked to the cavity via measurement-based (active) feedback but it is passively locked via the optical spring and the optical torsional spring effect. X is the measured output light field given by the following output equation:

$$X = \sqrt{\eta} x_{\text{out}} + \sqrt{1-\eta} x'_{\text{in}}, \quad x_{\text{out}} = x_{\text{in}} - \sqrt{\kappa} x,$$

where $\eta \in [0, 1]$ is the detection efficiency; note that x'_{in} is a fictitious vacuum field satisfying $\langle x_{\text{in}}'^2 \rangle = 1$, introduced to represent imperfect detection. Now assume $\kappa \gg \Omega$, meaning that the cavity mode changes much faster than the mechanical oscillator mode. This allows us to adiabatically eliminate the cavity mode, and the resulting equation of motion of the mechanical oscillator is given by

$$\begin{aligned}\dot{q} &= \Omega p, \\ \dot{p} &= -\left(\Omega + \frac{16\Delta g^2}{\kappa^2 + 4\Delta^2}\right)q - \gamma_m p + \sqrt{2\gamma_m} p_{\text{in}} - \frac{4g\kappa\sqrt{\kappa}}{\kappa^2 + 4\Delta^2}x_{\text{in}} + \frac{8g\Delta\sqrt{\kappa}}{\kappa^2 + 4\Delta^2}y_{\text{in}}, \\ X &= -\frac{8\Delta g\sqrt{\kappa\eta}}{\kappa^2 + 4\Delta^2}q - \sqrt{\eta} \cdot \frac{\kappa^2 - 4\Delta^2}{\kappa^2 + 4\Delta^2}x_{\text{in}} + \frac{4\Delta\kappa\sqrt{\eta}}{\kappa^2 + 4\Delta^2}y_{\text{in}} + \sqrt{1-\eta}x'_{\text{in}},\end{aligned}$$

where γ_m is the effective mechanical damping rate under feedback. Correspondingly, the effective temperature of the center-of-mass of the mechanical oscillator is reduced to $T\gamma_0/\gamma_m$. Here we introduce the following change of variables and parameters:

$$q = q' \sqrt{\frac{\Omega}{\omega_m}}, \quad p = p' \sqrt{\frac{\omega_m}{\Omega}}, \quad \omega_m = \sqrt{\frac{16\Delta g^2}{\kappa^2 + 4\Delta^2} \Omega + \Omega^2}.$$

The above system equations are then rewritten as

$$\begin{aligned}\dot{q} &= \omega_m p, \\ \dot{p} &= -\omega_m q - \gamma_m p + \sqrt{2\gamma_m} p_{\text{in}} - \frac{4g_m\kappa\sqrt{\kappa}}{\kappa^2 + 4\Delta^2}x_{\text{in}} + \frac{8g_m\Delta\sqrt{\kappa}}{\kappa^2 + 4\Delta^2}y_{\text{in}}, \\ X &= -\frac{8\Delta g_m\sqrt{\kappa\eta}}{\kappa^2 + 4\Delta^2}q - \sqrt{\eta} \cdot \frac{\kappa^2 - 4\Delta^2}{\kappa^2 + 4\Delta^2}x_{\text{in}} + \frac{4\Delta\kappa\sqrt{\eta}}{\kappa^2 + 4\Delta^2}y_{\text{in}} + \sqrt{1-\eta}x'_{\text{in}},\end{aligned}\tag{1}$$

where $g_m = g\sqrt{\Omega/\omega_m}$, and (q', p') have been again represented by (q, p) for simplifying the notation. This transformation of the mechanical resonance frequency also changes the autocorrelation of p_{in} to be $\langle p_{\text{in}}^2 \rangle = 2n_{\text{th}} + 1$, where $n_{\text{th}} = k_B T \gamma_0 / \gamma_m \hbar \omega_m$ is the unconditional thermal occupation under feedback. Note that, unlike the system considered by Meng et al., in [33], both of the optical noise components $(x_{\text{in}}, y_{\text{in}})$ contribute to the dynamics and output equations.

To generalize the model, we also consider the measurement of the phase quadrature as in Miki et al. [10]. The input-output relation for the phase quadrature is also expressed as

$$Y = \sqrt{\eta} y_{\text{out}} + \sqrt{1-\eta} y'_{\text{in}}, \quad y_{\text{out}} = y_{\text{in}} - \sqrt{\kappa} y.$$

Again, the equation above can be solved as follows:

$$Y = \frac{4g_m\kappa\sqrt{\eta\kappa}}{\kappa^2 + 4\Delta^2}q - \sqrt{\eta}\frac{4\kappa\Delta}{\kappa^2 + 4\Delta^2}x_{in} - \sqrt{\eta}\frac{\kappa^2 - 4\Delta^2}{\kappa^2 + 4\Delta^2}y_{in} + \sqrt{1 - \eta}y'_{in} \quad (2)$$

Furthermore, we can rewrite the Langevin equation for both quadratures in matrix form:

$$\begin{aligned} \frac{d\mathbf{r}}{dt} &= \mathbf{A}\mathbf{r} + \begin{pmatrix} 0 \\ w \end{pmatrix}, \\ X &= \mathbf{C}_X\mathbf{r} + v_X, \\ Y &= \mathbf{C}_Y\mathbf{r} + v_Y, \end{aligned} \quad (3)$$

where

$$\begin{aligned} \mathbf{A} &= \begin{pmatrix} 0 & \omega_m \\ -\omega_m & -\gamma_m \end{pmatrix}, & w &= \sqrt{2\gamma_m}p_{in} - \frac{4g_mk^{3/2}}{\kappa^2 + 4\Delta^2}x_{in} + \frac{8g_m\kappa^{1/2}\Delta}{\kappa^2 + 4\Delta^2}y_{in} \\ \mathbf{C}_X &= \begin{pmatrix} -\frac{8g_m\Delta\sqrt{\eta\kappa}}{\kappa^2 + 4\Delta^2} & 0 \end{pmatrix}, & v_X &= -\frac{\kappa^2 - 4\Delta^2}{\kappa^2 + 4\Delta^2}\sqrt{\eta}x_{in} + \frac{4\kappa\Delta}{\kappa^2 + 4\Delta^2}\sqrt{\eta}y_{in} + \sqrt{1 - \eta}x'_{in} \\ \mathbf{C}_Y &= \begin{pmatrix} \frac{4g_m\kappa\sqrt{\eta\kappa}}{\kappa^2 + 4\Delta^2} & 0 \end{pmatrix}, & v_Y &= -\frac{4\kappa\Delta}{\kappa^2 + 4\Delta^2}\sqrt{\eta}x_{in} - \frac{\kappa^2 - 4\Delta^2}{\kappa^2 + 4\Delta^2}\sqrt{\eta}y_{in} + \sqrt{1 - \eta}y'_{in} \end{aligned}$$

Also, $\mathbf{r} = (q, p)^T$ is the vector for position and momentum of the mechanical system; v_x, v_y describe the total sensing noise level given by the laser noise; w represents the total force noise due to the Brownian motion and the back-action. The variances for the stochastic noises in the Langevin equations are computed in the following way:

$$\begin{aligned} \langle w^2 \rangle &= 2\gamma_m(2n_{th} + 1) + \frac{16g_m^2\kappa}{\kappa^2 + 4\Delta^2}(2N_{th} + 1) \equiv \Gamma, \\ \langle wv_X \rangle &= \frac{4g_m\kappa\sqrt{\kappa\eta}}{\kappa^2 + 4\Delta^2}(2N_{th} + 1), \\ \langle wv_Y \rangle &= \frac{8g_m\Delta\sqrt{\kappa\eta}}{\kappa^2 + 4\Delta^2}(2N_{th} + 1), \\ \langle v_X^2 \rangle &= \langle v_Y^2 \rangle = (2\eta N_{th} + 1). \end{aligned}$$

Since the quantum system presented here only includes Gaussian noise, it is feasible to use the Kalman filter. The Kalman filter allows for the description of two type of outcomes: prediction and retrodiction. The former is understood as the conditional estimation in a causal manner, while the latter refers the conditional estimation in an anti-causal manner. $\vec{\mathbf{r}} = (\vec{q}, \vec{p})^T$ and $\mathbf{V} = \langle (r - \vec{\mathbf{r}})(r - \vec{\mathbf{r}})^T \rangle$ represent respectively the first and second moment for the predicted conditional state while $\overleftarrow{\mathbf{r}} = (\overleftarrow{q}, \overleftarrow{p})^T$ and $\mathbf{V}_E = \langle (r - \overleftarrow{\mathbf{r}})(r - \overleftarrow{\mathbf{r}})^T \rangle$ denote the first and second moment for retrodictive conditional state. The differential equation for the conditional variance \mathbf{V} corresponds to the following Riccati differential equation:

$$\frac{d\mathbf{V}}{dt} = \mathbf{A}\mathbf{V} + \mathbf{V}\mathbf{A}^T + \mathbf{N} - (\mathbf{V}\mathbf{C}_I^T + \mathbf{L}_I)M^{-1}(\mathbf{V}\mathbf{C}_I^T + \mathbf{L}_I)^T, \quad (4)$$

where I represents either X or Y . Furthermore, we define:

$$\begin{aligned} \mathbf{L}_I &= \begin{pmatrix} 0 \\ \langle wv_I \rangle \end{pmatrix}, \\ \mathbf{V} &= \begin{pmatrix} V_{11} & V_{12} \\ V_{12} & V_{22} \end{pmatrix}, & \mathbf{N} &= \begin{pmatrix} 0 & 0 \\ 0 & \langle w^2 \rangle \end{pmatrix} \\ M &= \langle v_I^2 \rangle = 2\eta N_{th} + 1 \end{aligned}$$

The solution for the stationary case $\dot{\mathbf{V}} = 0$ reads [10]:

$$\begin{aligned} V_{11} &= \frac{\gamma_I - \gamma_m}{\lambda_I} \\ V_{12} &= \frac{V_{11}^2}{2\omega_m}\lambda_I \\ V_{22} &= \frac{V_{11}}{2\omega_m^2}(2\omega_m(\omega_m + \Lambda_I) + \gamma_I V_{11}\lambda_I) \end{aligned} \quad (5)$$

The solution V_{11} (V_{22}) represents the predicted conditional variance for position (momentum). V_{12} is the predicted conditional covariance between position and momentum. Moreover, γ_I and ω_I are expressed as

$$\gamma_I = \sqrt{\gamma_m^2 - 2\omega_m(\omega_m + \Lambda_I) + 2\omega_I^2},$$

$$\omega_I = \sqrt[4]{\omega_m^4 + 2\Lambda_I\omega_m^3 + \Gamma\lambda_I\omega_m^2}.$$

Here, we can define the measurement rate $\lambda_I = \mathbf{C}_I \mathbf{C}_I^T M^{-1}$, which represents the inverse time scale to spatially resolve the zero-point motion. Also, as $\Lambda_I = \sqrt{\mathbf{C}_I \mathbf{C}_I^T \mathbf{L}_I^T \mathbf{L}_I} M^{-1}$ increases, the conditional position variance decreases, meaning that the q -squeezed state is more enhanced. The respective expressions for λ_I and Λ_I are given by

$$\begin{aligned}\lambda_X &= \frac{64g_m^2 \eta \kappa \Delta^2}{(2\eta N_{th} + 1)(\kappa^2 + 4\Delta^2)^2}, \\ \lambda_Y &= \frac{16g_m^2 \eta \kappa^3}{(2\eta N_{th} + 1)(\kappa^2 + 4\Delta^2)^2}, \\ \Lambda_X &= -\Lambda_Y = -\frac{32g_m^2 \eta \kappa^2 \Delta}{(\kappa^2 + 4\Delta^2)^2} \frac{2N_{th} + 1}{2\eta N_{th} + 1}.\end{aligned}$$

In the context of Meng et al. [33] where $N_{th} = 0$, $\Delta = 0$ and $I = Y$, we have $\lambda_Y = 4C\gamma_m\eta$. Here $C = 4g_m^2/(\kappa\gamma_m)$ is defined as cooperativity. We also see that if $\lambda_I = 0$ and $\Lambda_I = 0$, then $\omega_I = \omega_m$ and $\gamma_I = \gamma_m$, which recovers the initial values of the mechanical susceptibility.

To further explore the implications of the modified susceptibility, we obtain the PSD for the output signal $I = X$ or $I = Y$. We calculate the corresponding Fourier transformation $F(\omega) = \int_{-\infty}^{\infty} f(t)e^{i\omega t} dt$ for our Langevin equations in (3). Thus:

$$-i\omega \mathbf{r}(\omega) = \mathbf{A} \mathbf{r}(\omega) + \begin{pmatrix} 0 \\ w \end{pmatrix}.$$

Then, we have

$$q(\omega) = \frac{\omega_m}{F(\omega)} \left\{ \sqrt{2\gamma_m} p_{in}(\omega) - \frac{4g_m \kappa \sqrt{\kappa}}{\kappa^2 + 4\Delta^2} x_{in}(\omega) + \frac{8\Delta g_m \sqrt{\kappa}}{\kappa^2 + 4\Delta^2} y_{in}(\omega) \right\}$$

and

$$p(\omega) = -\frac{i\omega}{\omega_m} q(\omega) = \frac{-i\omega}{F(\omega)} \left\{ \sqrt{2\gamma_m} p_{in}(\omega) - \frac{4g_m \kappa \sqrt{\kappa}}{\kappa^2 + 4\Delta^2} x_{in}(\omega) + \frac{8\Delta g_m \sqrt{\kappa}}{\kappa^2 + 4\Delta^2} y_{in}(\omega) \right\},$$

where

$$F(\omega) = \omega_m^2 - i\gamma_m \omega - \omega^2.$$

The Fourier transformation for the linear measurement is expressed as

$$I(\omega) = \mathbf{C}_I \mathbf{r}(\omega) + v_I(\omega).$$

The symmetrized single-sided spectral density $S_{AB}(\omega)$ is defined through $2\pi\delta(\omega - \omega')S_{AB}(\omega) = \langle A(\omega)B^\dagger(\omega') + B^\dagger(\omega')A(\omega) \rangle$. For position and momentum, we obtain:

$$S_{qq}(\omega) = \frac{\omega_m^2 \Gamma}{|F(\omega)|^2}, \quad S_{pp}(\omega) = \frac{\omega^2 \Gamma}{|F(\omega)|^2}$$

and their variances

$$V_{qq} = \int_{-\infty}^{\infty} \frac{1}{2\pi} (S_{qq}(\omega)) d\omega = \Gamma/2\gamma_m, \quad V_{pp} = \int_{-\infty}^{\infty} \frac{1}{2\pi} (S_{pp}(\omega)) d\omega = \Gamma/2\gamma_m. \quad (6)$$

For $I = X, Y$, we calculate the PSD:

$$S_{II}(\omega) = C_I C_I^T S_{qq}(\omega) + S_{v_I v_I}(\omega) + \sqrt{C_I C_I^T} S_{qv_I}(\omega) + \sqrt{C_I C_I^T} S_{v_I q}(\omega)$$

Then,

$$S_{II}(\omega) = M \left(\frac{(-\omega^2 + \omega_I^2)^2 + \omega^2 \gamma_I^2}{(-\omega^2 + \omega_m^2)^2 + \omega^2 \gamma_m^2} \right)$$

or

$$S_{II}(\omega) = M \frac{|F'(\omega)|^2}{|F(\omega)|^2} \quad (7)$$

such that,

$$F'(\omega) = \omega_I^2 - i\gamma_I \omega - \omega^2$$

Again, when no measurement is performed, with $\lambda_I = 0$ and $\Lambda_I = 0$, then $F'(\omega) = F(\omega)$ and the PSD transforms into white noise. In this scenario, the physical significance of the matrix \mathbf{V} is lost.

2 Quantum estimation in frequency domain

In our analysis, we focus on the stationary behavior of the mechanical system. Therefore, we can obtain a quantum causal Wiener filter by examining the quantum causal Kalman filter in the frequency domain. We transform $F(\omega) = \int_{-\infty}^{\infty} f(t) e^{i\omega t} dt$. Then, from the differential equation of the first moment \vec{r} [43]:

$$\dot{\vec{r}} = \mathbf{A} \vec{r} + (\mathbf{V} \mathbf{C}_I^T + \mathbf{L}_I) M^{-1} (I - \mathbf{C}_I \vec{r}) \quad (8)$$

and using $\dot{\vec{r}}(t) = -i\omega \vec{r}(\omega)$, we simply obtain:

$$-i\omega \vec{r}(\omega) = \mathbf{A} \vec{r}(\omega) + (\mathbf{V} \mathbf{C}_I^T + \mathbf{L}_I) M^{-1} (I(\omega) - \mathbf{C}_I \vec{r}(\omega)).$$

We derive the steady-state solution for position and momentum in the frequency domain:

$$\begin{aligned} \vec{q}(\omega) &= \frac{1}{\sqrt{\lambda_I M}} \frac{(\omega_I^2 - \omega_m^2 - i\omega V_{11} \lambda_I) I(\omega)}{F'(\omega)}, \\ \vec{p}(\omega) &= \frac{1}{\sqrt{\lambda_I M} \omega_m} \frac{(-V_{11} \lambda_I \omega_m^2 - i\omega(\omega_I^2 - \omega_m^2 + V_{11}^2 \lambda_I^2 - V_{11} \lambda_I \gamma_I)) I(\omega)}{F'(\omega)}. \end{aligned} \quad (9)$$

This is exactly the quantum causal Wiener filter that estimates the position q and the momentum p from the measurement record I in the frequency domain. That is, we have:

$$\begin{aligned} \vec{q}(\omega) &= \vec{H}_q(\omega) I(\omega), \\ \vec{p}(\omega) &= \vec{H}_p(\omega) I(\omega), \end{aligned}$$

where

$$\vec{H}_q(\omega) = \frac{1}{\sqrt{\lambda_I M}} \frac{(\omega_I^2 - \omega_m^2) - i\omega(\gamma_I - \gamma_m)}{F'(\omega)}, \quad (10)$$

$$\vec{H}_p(\omega) = \frac{1}{\sqrt{\lambda_I M} \omega_m} \frac{-(\gamma_I - \gamma_m) \omega_m^2 - i\omega(\omega_I^2 - \omega_m^2 + (\gamma_I - \gamma_m)^2 - (\gamma_I - \gamma_m) \gamma_I)}{F'(\omega)}. \quad (11)$$

For $\Delta = 0$, $N_{th} = 0$ and $I = Y$, $\vec{H}_q(\omega)$ and $\vec{H}_p(\omega)$ are equivalent to the filter obtained by Meng et al [33]. We can see that the following relations hold:

$$\begin{aligned} V_{11} &= \int_{-\infty}^{\infty} \frac{1}{2\pi} (S_{qq}(\omega) - S_{\vec{q}\vec{q}}(\omega)) d\omega = V_{qq} - V_{\vec{q}\vec{q}}, \\ V_{22} &= \int_{-\infty}^{\infty} \frac{1}{2\pi} (S_{pp}(\omega) - S_{\vec{p}\vec{p}}(\omega)) d\omega = V_{pp} - V_{\vec{p}\vec{p}}, \\ V_{12} &= \int_{-\infty}^{\infty} \frac{1}{2\pi} \text{Re} (S_{qp}(\omega) - S_{\vec{q}\vec{p}}(\omega)) d\omega, \end{aligned} \quad (12)$$

where we used the following equations:

$$\int_{-\infty}^{\infty} \frac{1}{|F(\omega)|^2} d\omega = \frac{\pi}{\gamma_m \omega_m^2}, \quad \int_{-\infty}^{\infty} \frac{\omega^2}{|F(\omega)|^2} d\omega = \frac{\pi}{\gamma_m}.$$

3 Verification protocol

In order to experimentally verify the conditional variance \mathbf{V} , we use the retrodiction process in addition to the prediction process, using the quantum anti-causal Kalman filter. Since the unconditional variances of the true variables of q and p are experimentally unavailable, we perform a retrodiction-based verification technique [38] in the frequency domain to experimentally access the value of the conditional variance. For a Gaussian system, it is also possible to use the quantum Kalman filtering as well as the previous case for prediction [43]:

$$\dot{\overleftarrow{\mathbf{r}}} = -\mathbf{A}\overleftarrow{\mathbf{r}} + (\mathbf{V}_E \mathbf{C}_I^T - \mathbf{L}_I) M^{-1} (I - \mathbf{C}_I \overleftarrow{\mathbf{r}}) \quad (13)$$

As defined in the previous section, $\overleftarrow{\mathbf{r}} = (\overleftarrow{q}, \overleftarrow{p})^T$ represents the retrodictive conditional state and $\mathbf{V}_E = \langle (r - \overleftarrow{\mathbf{r}})(r - \overleftarrow{\mathbf{r}})^T \rangle$ is the retrodictive covariance matrix. The respective Riccati equation for retrodiction is expressed as given by Zhang et al. [43]

$$\frac{d\mathbf{V}_E}{dt} = -\mathbf{A}\mathbf{V}_E - \mathbf{V}_E \mathbf{A}^T + \mathbf{N} - (\mathbf{V}_E \mathbf{C}_I^T - \mathbf{L}_I) M^{-1} (\mathbf{V}_E \mathbf{C}_I^T - \mathbf{L}_I)^T \quad (14)$$

where $I = X$ or Y , and $M = \langle v_X^2 \rangle = \langle v_Y^2 \rangle = (2\eta N_{th} + 1)$. Here, \mathbf{V}_E is given by

$$\mathbf{V}_E = \begin{pmatrix} V_{E11} & V_{E12} \\ V_{E12} & V_{E22} \end{pmatrix}.$$

Considering the steady state $\dot{\mathbf{V}}_E = 0$, the covariance matrix satisfies the following equations:

$$\begin{aligned} -2\omega_m V_{E12} - V_{E11}^2 \lambda_I &= 0 \\ \omega_m (V_{E11} - V_{E22}) + (\gamma_m - V_{E11} \lambda_I) V_{E12} + V_{E11} \Lambda_I &= 0 \\ 2\gamma_m V_{E22} + 2\omega_m V_{E12} - (\sqrt{\lambda_I} V_{E12} - \Lambda_I / \sqrt{\lambda_I})^2 + \Gamma &= 0 \end{aligned}$$

After solving,

$$\begin{aligned} V_{E11} &= \frac{\gamma_I + \gamma_m}{\lambda_I} \\ V_{E12} &= -\frac{V_{E11}^2}{2\omega_m} \lambda_I \\ V_{E22} &= \frac{V_{E11}}{2\omega_m^2} (2\omega_m(\omega_m + \Lambda_I) + \gamma_I V_{E11} \lambda_I) \end{aligned} \quad (15)$$

The solution for the retrodictive conditional variance is similar to what was obtained before for prediction. The change in the direction of time for the estimation is reflected by the sign in front of the mechanical dissipation γ_m . As with the previous approach, we solved the differential equation for \mathbf{r} by introducing the Fourier transformation, $\overleftarrow{\mathbf{r}} = i\omega \overleftarrow{\mathbf{r}}$. However, it is important to note that the sign in the transformation is different due to the estimation going in the negative direction of time.

$$\dot{\overleftarrow{\mathbf{r}}} = -\mathbf{A}\overleftarrow{\mathbf{r}} + (\mathbf{V}_E \mathbf{C}_I^T - \mathbf{L}_I) M^{-1} (I - \mathbf{C}_I \overleftarrow{\mathbf{r}}) \quad (16)$$

We straightforwardly obtain

$$i\omega \overleftarrow{\mathbf{r}}(\omega) = -\mathbf{A}\overleftarrow{\mathbf{r}}(\omega) + (\mathbf{V}_E \mathbf{C}_I^T - \mathbf{L}_I) M^{-1} (I^\dagger(\omega) - \mathbf{C}_I \overleftarrow{\mathbf{r}}(\omega))$$

Then, calculating the value for position and momentum, we derive the following:

$$\begin{aligned} \overleftarrow{q}(\omega) &= \frac{1}{\sqrt{\lambda_I M}} \frac{(\omega_I^2 - \omega_m^2 + i\omega V_{E11} \lambda_I) I^\dagger(\omega)}{F'(\omega)^*} \\ \overleftarrow{p}(\omega) &= \frac{1}{\sqrt{\lambda_I M \omega_m}} \frac{(V_{E11} \lambda_I \omega_m^2 - i\omega(\omega_I^2 - \omega_m^2 + V_{E11}^2 \lambda_I^2 - V_{E11} \lambda_I \gamma_I)) I^\dagger(\omega)}{F'(\omega)^*} \end{aligned}$$

Again, we consider the mathematical representation of a filter applied over the measurement record.

$$\overleftarrow{q}(\omega) = \overleftarrow{H}_q(\omega)I^\dagger(\omega)$$

$$\overleftarrow{p}(\omega) = \overleftarrow{H}_p(\omega)I^\dagger(\omega)$$

then,

$$\overleftarrow{H}_q(\omega) = \frac{1}{\sqrt{\lambda_I M}} \frac{(\omega_I^2 - \omega_m^2) + i\omega(\gamma_I + \gamma_m)}{F'(\omega)^*} \quad (17)$$

$$\overleftarrow{H}_p(\omega) = \frac{1}{\sqrt{\lambda_I M \omega_m}} \frac{((\gamma_I + \gamma_m)\omega_m^2 - i\omega(\omega_I^2 - \omega_m^2 + (\gamma_I + \gamma_m)^2 - (\gamma_I + \gamma_m)\gamma_I))}{F'(\omega)^*} \quad (18)$$

In this case, we observe that the relationship between retrodictive conditional variance and unconditional variance differs from what was observed previously.

$$\begin{aligned} V_{E11} &= \int_{-\infty}^{\infty} \frac{1}{2\pi} (S_{\overleftarrow{q}\overleftarrow{q}}(\omega) - S_{qq}(\omega)) d\omega = V_{\overleftarrow{q}\overleftarrow{q}} - V_{qq} \\ V_{E22} &= \int_{-\infty}^{\infty} \frac{1}{2\pi} (S_{\overleftarrow{p}\overleftarrow{p}}(\omega) - S_{pp}(\omega)) d\omega = V_{\overleftarrow{p}\overleftarrow{p}} - V_{pp} \\ V_{E12} &= \int_{-\infty}^{\infty} \frac{1}{2\pi} \text{Re} (S_{\overleftarrow{q}\overleftarrow{p}}(\omega) - S_{qp}(\omega)) d\omega = V_{\overleftarrow{q}\overleftarrow{p}} - V_{qp}. \end{aligned} \quad (19)$$

By comparing the equation above (19) with the one obtained for predicted conditional variance (12), we have enough conditions for verification. The verification of the conditional variance can be derived from the following relations ((19) + (12))

$$\begin{aligned} \int_{-\infty}^{\infty} \frac{1}{2\pi} (S_{\overleftarrow{q}\overleftarrow{q}}(\omega) d\omega - S_{\overrightarrow{q}\overrightarrow{q}}(\omega) d\omega) &= V_{11} + V_{E11} \\ \int_{-\infty}^{\infty} \frac{1}{2\pi} (S_{\overleftarrow{p}\overleftarrow{p}}(\omega) d\omega - S_{\overrightarrow{p}\overrightarrow{p}}(\omega) d\omega) &= V_{22} + V_{E22} \\ \int_{-\infty}^{\infty} \frac{1}{2\pi} \text{Re} (S_{\overleftarrow{q}\overleftarrow{p}}(\omega) d\omega - S_{\overrightarrow{q}\overrightarrow{p}}(\omega) d\omega) &= V_{E12} + V_{12} \end{aligned} \quad (20)$$

When the measurement rate λ_I is larger than γ_m , we can affirm the relations as Rossi et. al.[38]:

$$V_{E11} = \frac{\gamma_I + \gamma_m}{\lambda_I} = V_{11} + 2\frac{\gamma_m}{\lambda_I} \approx V_{11} \quad (21)$$

Consequently,

$$\begin{aligned} V_{E12} &= -\frac{V_{E11}\lambda_I}{2\omega_m} \approx -\frac{V_{11}}{2\omega_m}\lambda_I = -V_{12} \\ V_{E22} &= \frac{V_{E11}}{2\omega_m^2}(2\omega_m(\omega_m + \Lambda_I) + \gamma_I V_{E11}\lambda_I) \approx \frac{V_{11}}{2\omega_m^2}(2\omega_m(\omega_m + \Lambda_I) + \gamma_I V_{11}\lambda_I) = V_{22} \end{aligned}$$

Then,

$$\begin{aligned} \int_{-\infty}^{\infty} \frac{1}{2\pi} (S_{\overleftarrow{q}\overleftarrow{q}}(\omega) d\omega - S_{\overrightarrow{q}\overrightarrow{q}}(\omega) d\omega) &\approx 2V_{11} \\ \int_{-\infty}^{\infty} \frac{1}{2\pi} (S_{\overleftarrow{p}\overleftarrow{p}}(\omega) d\omega - S_{\overrightarrow{p}\overrightarrow{p}}(\omega) d\omega) &\approx 2V_{22} \\ \int_{-\infty}^{\infty} \frac{1}{2\pi} (S_{\overleftarrow{q}\overleftarrow{p}}(\omega) d\omega - S_{\overrightarrow{q}\overrightarrow{p}}(\omega) d\omega) &\approx 0 \end{aligned} \quad (22)$$

To find the conditional variances in each case, we can use predictive and retrodictive filters along with the PSD of the measurement record ($I = X$ for our case):

$$\begin{aligned}
\int_{-\infty}^{\infty} \frac{1}{2\pi} (|\overleftarrow{H}_q(\omega)|^2 - |\overrightarrow{H}_q(\omega)|^2) S_{II}(\omega) d\omega &\approx 2V_{11} \\
\int_{-\infty}^{\infty} \frac{1}{2\pi} (|\overleftarrow{H}_p(\omega)|^2 - |\overrightarrow{H}_p(\omega)|^2) S_{II}(\omega) d\omega &\approx 2V_{22} \\
\int_{-\infty}^{\infty} \frac{1}{2\pi} \text{Re} (\overleftarrow{H}_q(\omega) \overleftarrow{H}_p^*(\omega) - \overrightarrow{H}_q(\omega) \overrightarrow{H}_p^*(\omega)) S_{II}(\omega) &\approx 0
\end{aligned} \tag{23}$$

To ensure consistency with the previous report [33], we consider the following situation. When the measurement rate is larger than mechanical dissipation ($\lambda_I \gg \gamma_m$), the filters for prediction and retrodiction can be approximated as

$$\begin{aligned}
\overrightarrow{H}_q(\omega) &\approx \overleftarrow{H}_q^*(\omega) \\
\overrightarrow{H}_p(\omega) &\approx -\overleftarrow{H}_p^*(\omega).
\end{aligned}$$

These are the same conditions as obtained in the previous research [33]. Here, the time symmetry $t \rightarrow -t$ is restored in the quantum filters such that $\overrightarrow{q}(\omega) = \overleftarrow{q}^*(\omega)$ and $\overrightarrow{p}(\omega) = -\overleftarrow{p}^*(\omega)$. The minus sign in the momentum is a result of the time variation.

4 The auxiliary measurement

In order to characterize the optomechanical interaction, we measured the resonance frequency of the optically trapped pendulum with varying detuning. The resonance frequency of the optically trapped pendulum is given by

$$\omega_m = \sqrt{\frac{8\hbar G^2 n_c \delta}{(1 + 4\delta^2)\kappa m}}. \quad (24)$$

The resonance ω_m was identified by measuring the transfer function as shown in Fig. 5. This auxiliary measurement was performed with a relatively small incident laser power of 3 mW, compared to the main measurement of 30 mW in the main text. Thus, the results are compensated for the power difference by multiplying the measured resonance by the square root of the power ratio shown as cyan dots in Fig. 6 (a).

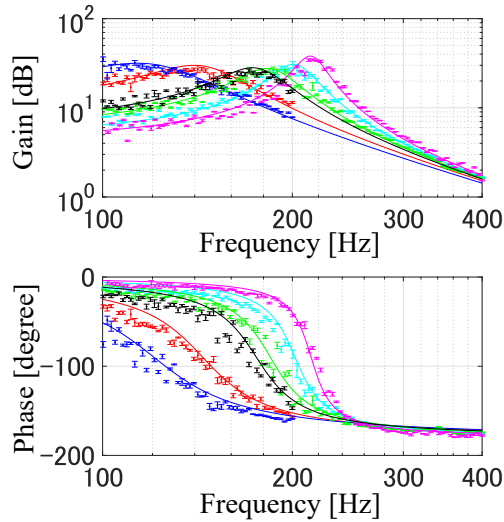


Figure 5: (Color online) The gain and phase plots of the transfer function of the optically trapped mechanical pendulum.

5 Main data in the time domain

In order to characterize the optomechanical interaction, we measured the resonance frequency of the optically trapped pendulum with varying detuning. The resonance frequency of the optically trapped pendulum is given by

$$\omega_m = \sqrt{\frac{8\hbar G^2 n_c \delta}{(1 + 4\delta^2)\kappa m}}. \quad (25)$$

As explained in the main text, the cavity length was detuned from resonance such that the pendulum's resonance ($\omega_m/2\pi$) increases to 280 Hz. Because of the nonlinearity of the optical spring with respect to δ , this leads to a mean value for the detuning of roughly $0.03 \times \kappa$ or $1.2 \times \kappa$. To determine the detuning based on the optical spring effect, we analyze the variation of the optically trapped pendulum's resonance over time. As shown in Fig. 6 (b), the raw data is bandpass filtered around the resonance from 170 Hz to 360 Hz, and then the number of zero crossings is counted in order to estimate its instantaneous resonance frequency. Next, the analyzed resonance is low pass filtered with a cutoff frequency of 8.2 Hz, and divided into 25 time bins. The result agrees well with the theoretical model for small detuning, as shown in Fig. 6 (c). The result of the counting is further divided into three bins of different resonance frequency values, and then averaged for each bin. Fitting the averaged

data with respect to detuning, to the theoretical model shown in Fig. 6 (a), the mean value of the detuning is determined to be $\Delta = 0.0292(4) \times \kappa$. Here, we should note that the temperature for the confined mode is relatively high compared to the theoretical prediction given by $T\gamma_0(\omega_m)/\gamma_m$, where T is the room temperature. We mainly attribute this to fluctuations of the resonance frequency, namely, the detuning, as shown in Fig. 6. As a result, the quantum cooperativity decreases by a factor of 10. Furthermore, it also decreases by a factor of 4 due to mode mixing between the pendulum mode and the dissipative pitching mode [39, 46]. Thus, compared to the case without optical spring, the quantum cooperativity of the current experiment is enhanced by a factor of $(\omega_m/\Omega)/10/4 = 1.5$.

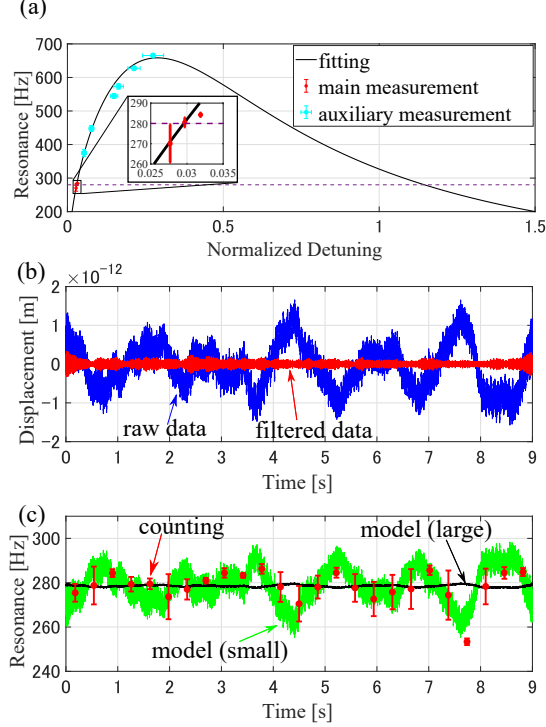


Figure 6: (Color online) The fluctuation of the cavity detuning in the case of the data with the higher mode temperature of 11 mK. (a) Optomechanical interaction characterized by the optical spring effect. The data of the main measurement (red) is obtained from the red dots in (c). (b) The calibrated raw data (blue) and the bandpass filtered data from 170 Hz to 360 Hz (red). (c) Variation of the resonance over time. The red dots are obtained by the frequency counting from the bandpass filtered data. The two curves show the model resonance frequency calculated by applying the raw data to the equation of the optical spring for the small detuning (green) and the large detuning (black), respectively.

6 Validity of approximation for verification

Based on the mean value given by the uncertainty in each optomechanical parameter, the theoretical value for our conditional variances are given by $V_{11} = 1242$, $V_{22} = 7850$, and $V_{12} = 2386$, respectively.

Then, we examine the validity of the approximation that can be made between the conditional variances for prediction and retrodiction as given by (21):

$$\begin{aligned} \text{Position Variance Verification} &= V_{11} + V_{E11} \\ &= 2V_{11} + 2\frac{\gamma_m}{\lambda_X} \end{aligned}$$

Since $\gamma_m/\lambda_X = 1.27$ is smaller compared to the value of V_{11} , we can approximate $V_{E11} + V_{11} \approx 2V_{11}$.

For the momentum verification, this approximation can also be extended:

$$\begin{aligned} \text{Momentum Variance Verification} &= V_{22} + V_{E22} \\ &= \frac{2V_{11} + 2\gamma_m/\lambda_X}{2\omega_m^2} (2\omega_m(\omega_m + \Lambda_X)) + \frac{\gamma_X}{2\omega_m^2} (V_{11}^2 + (V_{11} + 2\gamma_m/\lambda_X)^2)\lambda_X \end{aligned}$$

Similarly, we can conclude that $V_{E22} + V_{22} \approx 2V_{22}$.

Specifically, we have the following values for the relative error in each approximation:

$$\begin{aligned} \frac{(V_{E11} + V_{11}) - 2V_{11}}{2V_{11}} \times 100\% &= 0.1\% \\ \frac{(V_{E22} + V_{22}) - 2V_{22}}{2V_{22}} \times 100\% &= 0.2\% \end{aligned}$$

These values are smaller than the ones we obtained for the modeling error ($\approx 10\%$). Therefore, we can consider our approximation as appropriate for each case.

We are thankful Seth B. Cataño-Lopez for help with the manuscript and discussions. We thank Keiichi Edamatsu and Daisuke Miki for discussions. We thank Chao Meng for answering our questions. This research is supported by JSPS KAKENHI Grant No. 15617498 and JST FORESTO Grant No. JPMJFR202X.

References

- [1] B. P. Abbott et al. (LIGO Scientific Collaboration and Virgo Coaboration), *Phys. Rev. Lett.* **116**, 061102 (2016).
- [2] B. P. Abbott et al. (LIGO Scientific Collaboration and Virgo Coaboration), *Phys. Rev. Lett.* **119**, 161101 (2017).
- [3] M. Aspelmeyer, T. J. Kippenberg, and F. Marquardt, *Rev. Mod. Phys.* **86**, 1391 (2014).
- [4] V. B. Braginsky, *Sov. Phys. JETP* **26**, 831–834 (1968).
- [5] V. B. Braginsky and F. Y. Khalili, *Quantum Measurement* (Cambridge University Press, Cambridge, England, 1995).
- [6] D. J. Wilson, V. Sudhir, N. Piro, R. Schilling, A. Ghadimi, and T. J. Kippenberg, *Nature* **524**, 325–329 (2015).
- [7] M. Rossi, D. Mason, J. Chen, Y. Tsaturyan, and A. Schliesser, *Nature* **563**, 53–58 (2018).
- [8] C. Whittle et al., *Science* **372**, 1333–1336 (2021)
- [9] H. Mller-Ebhardt, H. Rehbein, R. Schnabel, K. Danzmann, and Y. Chen, *Phys. Rev. Lett.* **100**, 013601 (2008).
- [10] D. Miki, N. Matsumoto, A. Matsumura, T. Shichijo, Y. Sugiyama, K. Yamamoto, and N. Yamamoto, *Phys. Rev. A*, **107**, 032410 (2023)
- [11] V. B. Braginsky, and F. Ya. Khalili, *Phys. Lett. A* **257**, 241–246 (1999).
- [12] A. H. Ghadimi, S. A. Fedorov, N. J. Engelsen, M. J. Beryhi, R. Schilling, D. J. Wilson, T. J. Kippenberg, *Science* **360**, 764–768 (2018).
- [13] S. B. Cataño-Lopez, J. G. Santiago-Condori, K. Edamatsu, and N. Matsumoto, *Phys. Rev. Lett.* **124**, 221102 (2020).
- [14] G. D. Cole, W. Zhang, M. J. Martin, J. Ye, and M. Aspelmeyer, *Nature Photonics* **7**, 644–650 (2013).
- [15] R. Penrose, *Gen. Rel. Grav.* **28**, 581–600 (1996).

- [16] L. Diósi, *Phys. Lett. A* **120**, 377-381 (1987).
- [17] A. Bassi, A. Großardt and H. Ulbricht, *Class. Quantum Grav.* **34**, 193002 (65pp) (2017).
- [18] D. Kafri, J.M. Taylor, and G. J. Milburn, *Class. Quantum Grav.* **16**, 065020 (2014).
- [19] S. Kanno, J. Soda, and J. Tokuda, *Phys. Rev. D* **103**, 044017 (2021).
- [20] S. Kanno, J. Soda, and J. Tokuda, *Phys. Rev. D* **104**, 083516 (2021).
- [21] C. Moller, *Les Theories Relativistes de la Gravitation Colloques Internationaux CNRX 91 ed A Lichnerowicz and M-A Tonnelat (Paris: CNRS) (1962).*
- [22] L. Rosenfeld, *Nucl. Phys.* **40**, 353 (1963).
- [23] H. Yang, H. Miao, Da-Shin Lee, B. Helou, and Y. Chen, *Phys. Rev. Lett.* **110**, 170401 (2013).
- [24] P. W. Graham, D. E. Kaplan, J. Mardon, S. Rajendran, and W. A. Terrano *Phys. Rev. D*, **93**, 075029 (2016).
- [25] D. Carney, A. Hook, Z. Liu, J. M. Taylor, and Y. Zhao, *New Journal of Physics*, **23**, (2021).
- [26] D. Carney, *et al.*, *Quantum Sci. Technol.* **6**, 024002 (2021).
- [27] C. M. DeWitt and D. Rickles, *The Role of Gravitation in Physics: Report from the 1957 Chapel Hill Conference* (2011).
- [28] C. Marletto and V. Vedral, *Phys. Rev. Lett.* **119**, 240402 (2017).
- [29] S. Bose, A. Mazumdar, G. W. Morley, H. Ulbricht, M. Toroš, M. Paternostro, A. A. Geraci, P. F. Barker, M.S. Kim, and G. Milburn, *Phys. Rev. Lett.* **119**, 240401 (2017).
- [30] A. Belenchia, R. Wald, F. Giacomini, E. Castro-Ruiz, C. Brukner, M. Aspelmeyer, *Phys. Rev. D* **98**, 126009 (2018).
- [31] D. Miki, A. Matsumura, and K. Yamamoto, [arXiv:2311.00563](https://arxiv.org/abs/2311.00563).
- [32] C. Meng, G. A. Brawley, J. S. Bennett, and W. P. Bowen, *Phys. Rev. Lett.* **125**, 0604 (2020).
- [33] C. Meng, G. A. Brawley, S. Khademi, E. M. Bridge, J. S. Bennett, and W. P. Bowen, *Science Advances*, **8(21)**, eabm7585 (2022).
- [34] N. Wiener, *Extrapolation, Interpolation, and Smoothing of Stationary Time Series* (The MIT Press, 1964).
- [35] V.B. Braginsky and A.B. Manukin, *Sov. Phys. JETP*, **25**, 653, (1967).
- [36] F. Ya. Khalili, *Phys. Lett. A*, **288**, 251-256 (2001).
- [37] V. B. Braginsky and F. Khalili, *Phys. Lett. A*, **257**, 241 (1999).
- [38] M. Rossi, D. Mason, J. Chen, and A. Schliesser, *Phys. Rev. Lett*, **123**, 163601 (2019)
- [39] N. Matsumoto, S. B. Cataño-Lopez, M. Sugawara, S. Suzuki, N. Abe, K. Komori, Y. Michimura, Y. Aso, and Keiichi Edamatsu, *Phys. Rev. Lett.*, **122**, 071101 (2019).
- [40] T. Westphal, H. Hepach, J. Pfaff. et al., *Nature* **591**, 225-228 (2021).
- [41] N. Matsumoto, K. Komori, S. Ito, Y. Michimura, and Y. Aso, *Phys. Rev. A* **94**, 033822 (2016).
- [42] C. K. Law, *Phys. Rev. A* **51**, 2537 (1995).
- [43] J. Zhang and K. Mølmer, *Phys. Rev. A*, **96**, 062131 (2017)
- [44] H. I. Nurdin and N. Yamamoto, *Linear Dynamical Quantum Systems* (Springer, New York, 2017).
- [45] P. R. Saulson, *Phys. Rev. D*, **42**, 2437 (1990).

- [46] Y. Sugiyama, T. Shichijo, N. Matsumoto, A. Matsumura, D. Miki, and K. Yamamoto, [Phys. Rev. A, **107**, 033515 \(2023\)](#).
- [47] N. Matsumoto, Y. Michimura, Y. Aso, and K. Tsubono, [Opt. Express **22**, 12915 \(2014\)](#).
- [48] P. Welch, [IEEE Transactions on Audio and Electroacoustics, **15**, 70-73, \(1967\)](#).
- [49] T. Shichijo, N. Matsumoto, A. Matsumura, D. Miki, Y. Sugiyama, and K. Yamamoto, [arXiv:2303.04511](#)